ACS Partner Journal
PRECISION CHEMISTRY
pubs.acs.org/PrecisionChem
Article

Facile Microwave-Assisted Synthesis of 2D Imine-Linked Covalent Organic Frameworks for Exceptional Iodine Capture

Ziad Alsudairy, Normanda Brown, Chongqing Yang, Songliang Cai, Fazli Akram, Abrianna Ambus, Conrad Ingram, and Xinle Li*

Cite This: *Precis. Chem.* 2023, 1, 233−240
Read Online
ACCESS | Metrics & More | Article Recommendations | Supporting Information

ABSTRACT: Covalent organic frameworks (COFs) have emerged as auspicious porous adsorbents for radioiodine capture. However, their conventional solvothermal synthesis demands multiday synthetic times and anaerobic conditions, largely hampering their practical use. To tackle these challenges, we present a facile microwave-assisted synthesis of 2D imine-linked COFs, Mw-TFB-BD-X, (X = $-CH_3$ and $-OCH_3$) under air within just 1 h. The resultant COFs possessed higher crystallinity, better yields, and more uniform morphology than their solvothermal counterparts. Remarkably, Mw-TFB-BD-CH_3 and Mw-TFB-BD-OCH_3 exhibited exceptional iodine adsorption capacities of 7.83 g g^{-1} and 7.05 g g^{-1}, respectively, placing them among the best-performing COF adsorbents for static iodine vapor capture. Moreover, Mw-TFB-BD-CH_3 and Mw-TFB-BD-OCH_3 can be reused 5 times with no apparent loss in the adsorption capacity. The exceptionally high iodine adsorption capacities and excellent reusability of COFs were mainly attributed to their uniform spherical morphology and enhanced chemical stability due to the in-built electron-donating groups, despite their low surface areas. This work establishes a benchmark for developing advanced iodine adsorbents that combine fast kinetics, high capacity, excellent reusability, and facile rapid synthesis, a set of appealing features that remain challenging to merge in COF adsorbents so far.

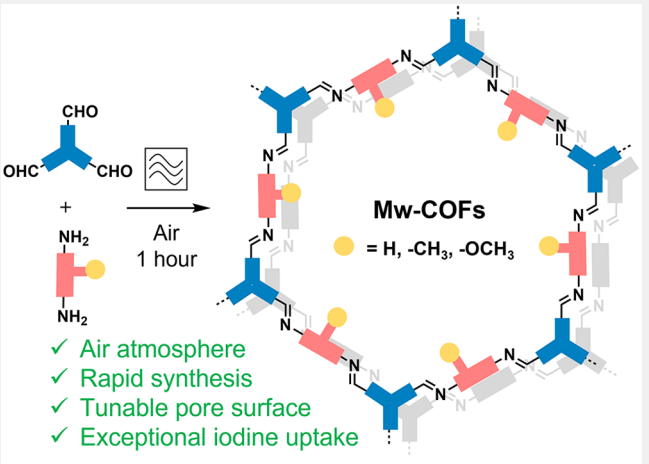

KEYWORDS: *covalent organic frameworks, microwave-assisted synthesis, isoreticular materials, radioactive iodine sequestration, charge transfer*

INTRODUCTION

Nuclear power provides approximately 10% of the world's electricity, but the disposal of nuclear waste containing hazardous radioactive species poses a significant threat to the environment and all living beings.[1] One of the most concerning pollutants is radioactive iodine, principally ^{129}I and ^{131}I, due to the extremely long half-life (~15.7 million years for ^{129}I) and potential health risks (carcinogenic effect of ^{131}I).[2] Therefore, it is of paramount importance to develop effective methods for radioactive iodine sequestration to ensure global environmental safety. Of the many radioiodine removal techniques, adsorptive removal is deemed a viable solution due to its low cost, simplified design, ease of operation, and high efficiency. However, the current adsorptive materials like activated charcoals and silver-exchanged zeolites have low practical adsorption capacity (0.10−0.31 g g^{-1}), high replenishment temperature, and high industrialization cost, making them unsuitable for practical iodine capture.[3] Hence, developing advanced adsorbents featuring high capacity, rapid kinetics, and excellent durability becomes an imperative necessity. Two categories of porous adsorbents have been developed. The first, amorphous porous adsorbents, such as porous carbons,[4] mesoporous silicas,[5] and porous organic polymers (POPs),[6] have irregular and discontinuous pore channels, which result in pore blockage and impede the establishment of clear-cut structure−function relationships.[7] The second category, crystalline porous adsorbents like silver-exchanged zeolites,[8] and metal−organic frameworks (MOFs),[9] typically exhibit low gravimetric adsorption owing to their intrinsic metallic components. Therefore, developing advanced iodine porous adsorbents that feature low density, high adsorption capacity, and great stability, along with precise

Received: January 10, 2023
Revised: March 5, 2023
Accepted: March 6, 2023
Published: March 17, 2023

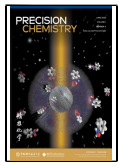

https://doi.org/10.1021/prechem.3c00006
Precis. Chem. 2023, 1, 233−240

Scheme 1. (A) Facile Microwave-Assisted Synthesis of Mw-TFB-BD-X COFs (X = $-CH_3$ and $-OCH_3$) under Air in 1 h and Space-Filling Models of (B) Mw-TFB-BD-CH_3 and (C) Mw-TFB-BD-OCH_3 with Layers Arranged in an Eclipsed Stacking Mode

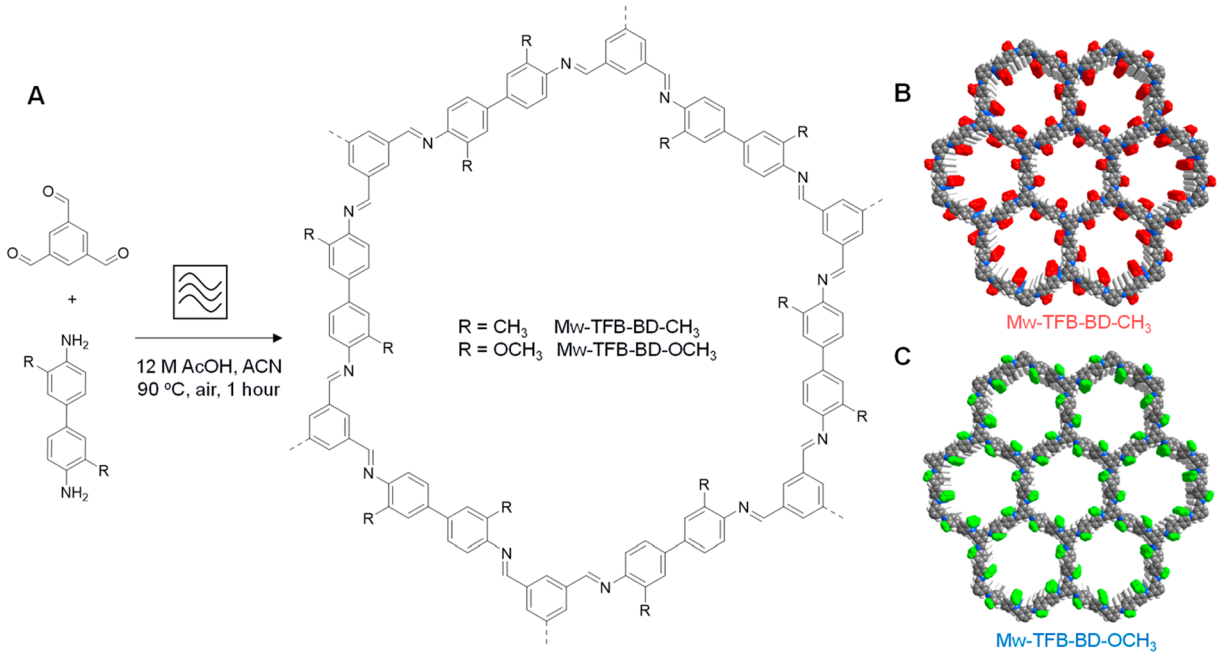

structural tunability and rational performance improvement is much desired.[10−12]

Covalent organic frameworks (COFs) are a novel class of crystalline porous polymers that precisely stitch organic monomers into two- or three-dimensional (2D or 3D) periodic networks.[13] Since their initial report in 2005, COFs have been the hot topic of immense research due to their salient structural merits of ultralight character, high crystallinity, permanent porosity, and customizable structures, which underpin their broad applications in gas storage, molecular separation, sensing, cancer therapy, optoelectronics, catalysis, energy storage, environmental remediation, etc.[14−18] Among these applications, radionuclide sequestration by COFs has aroused tremendous research interest in recent years.[7] The first study of using COFs for radioiodine capture dates back to 2017.[19] Since then, COFs have emerged as competent adsorbents for iodine capture by virtue of large surface areas, accessible 1D nanochannels, extraordinary framework tunability, superb stability, and abundant periodically arranged affinity sites such as imine,[20] thiophene,[21] hydrazide,[22] phosphine,[23] amine,[24] and cationic units,[25] giving rise to numerous COF adsorbents with high capacity, fast kinetics, and full reusability (see Table S1 for an overview of efficient COF adsorbents).[26] Notably, Han's group developed (2021) a series of ionic COFs (iCOFs) using a "post-modification of multivariate COFs" strategy.[27] The obtained iCOF-AB-50 exhibited a record-high static iodine adsorption capacity of 10.21 g g^{-1}. Different from the above postmodification method, Fang's group reported (2021) a *de novo* synthesis of two tetrathiafulvalene-based imine-linked COFs for static iodine adsorption and achieved a high iodine capture capacity of 8.19 g g^{-1}.[28] Apart from the dominant COF powders as adsorbents, Verduzco's group fabricated six macroscopic COF aerogels with high iodine capture capacities of up to 7.7 g g^{-1}, outperforming its powder counterpart.[29] Despite remarkable strides, the synthesis of COF adsorbents predominantly requires long reaction times (typically 3 days), vacuum conditions, cumbersome procedures (e.g., freeze−pump−thaw), and synthetically arduous monomers (e.g., 2,3,6,7-tetra(4-formylphenyl)tetrathiafulvalene[28] and 1,3,5,7-tetrakis-(4-aminophenyl)-adamantane[30]), severely constraining the full exploitation of COFs in radioiodine capture. As such, developing a facile, rapid, and efficient synthetic route to high-performing COF adsorbents using readily available monomers is greatly demanded but remains scarcely explored.

On the other hand, the rapid synthesis of COFs using alternate energy sources, such as mechanochemistry,[31] electron beam,[32] and sonochemistry,[33] has triggered enormous scientific attention over the past decade, since the sluggish solvothermal synthesis creates considerable hurdles for their further applications.[34] Among them, microwave-assisted synthesis has gained increasing popularity due to its intrinsic advantages over conventional solvothermal methods, such as higher yield, lower energy consumption, and improved physicochemical properties of products.[35] Cooper's group first (2009) applied microwave heating in the synthesis of prototypical boronate ester-linked COFs, exhibiting a 200-fold faster reaction rate than the solvothermal method.[36] Since then, tremendous scientific efforts have been devoted to the microwave-assisted synthesis of COFs bearing a wide array of linkages, such as β-ketoenamine, imine, triazine, imide, and aryl ether. More importantly, the microwave-synthesized COFs exhibited superior performance to their conventional solvothermal counterparts in gas separation, water purification, CO_2 uptake, and catalysis, underlining the advantages and great prospects of microwave-assisted synthesis.[37] Thus, we envisage that microwave-assisted synthesis may provide a feasible solution to overcome the limitations associated with the predominant solvothermal synthesis of COF adsorbents. To the best of our knowledge, the microwave-assisted synthesis of COF adsorbents for iodine capture remains untapped thus far.

https://doi.org/10.1021/prechem.3c00006
Precis. Chem. 2023, 1, 233−240

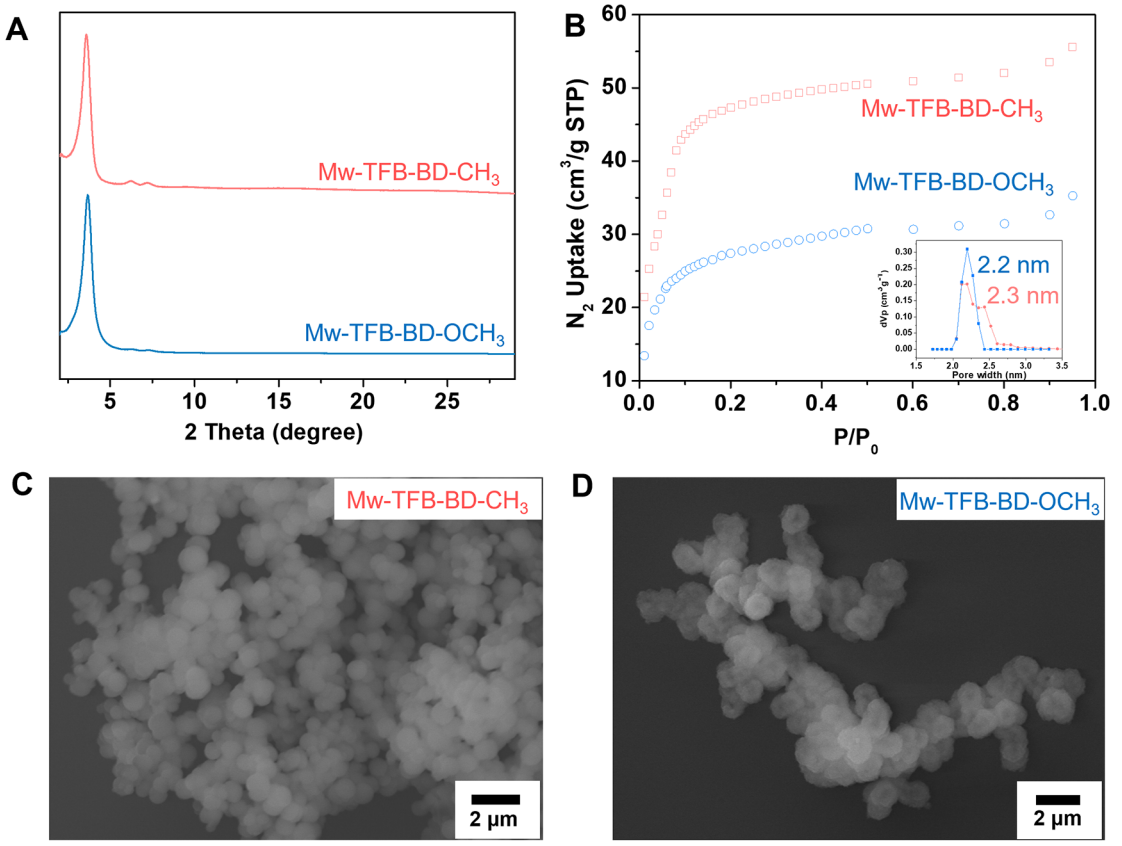

Figure 1. Characterizations of Mw-TFB-BD-CH_3 and Mw-TFB-BD-OCH_3. (A) PXRD patterns; (B) N_2 adsorption isotherms. Inset shows the pore size distributions; (C) Scanning electron micrograph of Mw-TFB-BD-CH_3; (D) Scanning electron micrograph of Mw-TFB-BD-OCH_3.

In this work, we for the first time report a facile and rapid microwave-assisted synthesis of COF adsorbents for efficient iodine capture. Two isoreticular 2D imine-linked COFs (termed Mw-TFB-BD-X COFs, X = $-CH_3$ and $-OCH_3$, Scheme 1) were rapidly synthesized under air and microwave heating by the Schiff-base condensation between 1,3,5-triformylbenzene (TFB) and substituted benzidine (BD) derivatives. The subtle change of functional groups on the pore walls of COFs led to different physicochemical properties including crystallinity, porosity, crystallite size, and thermal/chemical stability. Notably, the Mw-COFs exhibited enhanced crystallinity, high yields, and uniform morphology compared to their solvothermal counterparts. When implemented as adsorbents for static iodine vapor capture at 75 °C under ambient pressure, the 1-h-made Mw-TFB-BD-CH_3 and Mw-TFB-BD-OCH_3 COFs exhibited outstanding iodine adsorption capacities of 7.83 g g^{-1} and 7.05 g g^{-1}, respectively, exceeding those of nonfunctionalized Mw-TFB-BD, the solvothermal counterparts, and most reported COF adsorbents. In addition, Mw-TFB-BD-CH_3 and Mw-TFB-BD-OCH_3 retained high iodine adsorption capacities even after 5 successive adsorption−desorption cycles.

RESULTS AND DISCUSSION

The quality of imine-linked COFs is influenced by a variety of factors, including both intrinsic and extrinsic factors.[38−40] Intrinsic factors, such as the pendant functional groups (e.g., hydroxyl and fluorine) in monomers, can exquisitely control the noncovalent interactions like van der Waals/dipolar force, and interlayer stacking in 2D COFs, thereby affecting their physicochemical properties, including crystallinity, porosity, morphology, and thermal/chemical stability.[41] For example, the introduction of electron-donating methoxy and methyl groups into the skeleton of 2D imine COFs has been shown to reinforce their chemical stability.[42,43] Intrinsic factors like synthetic conditions are also essential for the quality of imine-linked COFs. The choice of solvent can profoundly affect the crystallinity and morphology of COFs. Acetonitrile is a proven solvent to afford highly crystalline imine COFs with uniform spherical morphologies.[44,45] With these considerations in mind, we synthesized two 2D imine-linked COFs with electron-donating groups in their skeletons (Mw-TFB-BD-CH_3 and Mw-TFB-BD-OCH_3, Scheme 1) under microwave heating and air. To obtain the optimal crystallization condition, we systemically tweaked the solvent, catalyst concentration, and reaction temperature, which exerted a profound effect on the crystallinity of COFs. We observed that the classic organic solvents such as mesitylene and dioxane did not produce highly crystalline products, whereas acetonitrile significantly enhanced the crystallinity of obtained COFs. Moreover, increasing the concentration of acetic acid catalyst from 3 to 12 M improved the crystallinity dramatically. At last, optimal temperature was achieved at 90 °C among three tested reaction temperatures (70 °C, 90 °C, and 110 °C) (see the screened conditions in Figures S1 and S2).

Under the optimized condition, TFB (0.08 mmol) and substituted benzidine (0.12 mmol), i.e., 3,3′-dimethylbenzidine (BD-CH_3) and 3,3′-dimethoxylbenzidine (BD-OCH_3) were mixed in acetonitrile (1 mL) in a 5 mL microwave vial. The reaction mixture was completely dissolved under sonication.

https://doi.org/10.1021/prechem.3c00006
Precis. Chem. 2023, 1, 233−240

Subsequently, aqueous acetic acid (12 M, 0.3 mL) catalyst was added, resulting in the immediate formation of yellow precipitates. The microwave vial was sealed under air, placed in a Biotage Initiator microwave reactor (Figure S3), and stirred at 90 °C for 1 h. To highlight the crucial role of functional groups on COFs as well as the advantages of microwave-assisted synthesis, we deliberately prepared the nonfunctionalized Mw-TFB-BD and their solvothermal counterparts using traditional synthetic methods as control samples.

The crystallinity of COFs prepared via microwave and conventional solvothermal routes was confirmed by powder X-ray diffraction (PXRD) analysis. Both high crystallinity and yields were achieved for all Mw-COFs under microwave heating (90 °C, air, 1 h, Figures S4−S6). In contrast, the conventional solvothermal method failed to produce any precipitate for TFB-BD-CH_3 in 1 h at 90 °C (Figure S4). Extending the reaction time to 72 h led to crystalline TFB-BD-CH_3 with a comparable yield (termed oven-TFB-BD-CH_3, Figure S7). Similarly, TFB-BD-OCH_3 and TFB-BD synthesized via the conventional solvothermal route revealed minimal crystallinity in 1 h and moderate crystallinity after 72 h (termed oven-TFB-BD-OCH_3 and oven-TFB-BD, Figures S5−S7). The marked difference in crystallinity and yields underscored the advantages of microwave-assisted synthesis over the conventional solvothermal method in making COFs, which simultaneously accelerated the rates of both imine formation and error correction during COF formation.[46] Furthermore, to assess the feasibility of large-scale synthesis under microwave irradiation, we scaled up the synthesis of Mw-TFB-BD-CH_3 by 10-fold. The COF synthesis proceeded smoothly with a high yield of 90%, producing over 300 mg of highly crystalline COF within 1 h (Figure S8). At the optimal synthesis condition, the PXRD pattern of obtained Mw-TFB-BD-CH_3 revealed four discernible peaks at 2θ = 3.55°, 6.18°, 7.19°, and 24.5°, corresponding to the (100), (110), (200), and (001) reflection planes, respectively (Figure 1 A, red curve). Likewise, the PXRD pattern of Mw-TFB-BD-OCH_3 indicated main diffraction peaks at 2θ = 3.59° and 24.5°, assignable to the (100) and (001) reflection planes, respectively (Figure 1 A, blue curve). The similar powder patterns implied the isoreticular nature of the two COFs. Importantly, the experimental PXRD patterns were in good agreement with simulated ones of the eclipsed AA stacked model (Figures S9 and S10), indicating Mw-TFB-BD-CH_3/-OCH_3 COFs adopt a 2D honeycomb topology with layers stacked in an eclipsed mode (Scheme 1). Moreover, Pawley refinements were performed on the experimental powder patterns, and the refined PXRD curves reproduced the experimentally observed ones, as evident by the small agreement factors (R_{WP} = 2.05%, R_P = 1.61% for Mw-TFB-BD-CH_3 and R_{WP} = 2.20%, R_P = 1.81% for Mw-TFB-BD-OCH_3). The formation of imine bonds was confirmed by Fourier transform infrared (FT-IR) and X-ray photoelectron spectroscopy (XPS) analysis. FT-IR spectra of Mw-TFB-BD-CH_3 and Mw-TFB-BD-OCH_3 showed characteristic imine C═N stretch at 1623 and 1617 cm^{-1}, respectively, indicative of the successful Schiff-base reaction (Figure S11). In addition, the N 1s XPS spectra of Mw-TFB-BD-CH_3 and Mw-TFB-BD-OCH_3 showed intense binding energy peaks at 398.3 and 398.2 eV, respectively (Figure S12), which were attributed to the C═N nitrogen.

The permanent porosity and surface area of activated Mw-COFs were assessed by nitrogen adsorption isotherms at 77 K (Figure 1B). Brunauer−Emmett−Teller (BET) surface areas of Mw-TFB-BD-CH_3 and Mw-TFB-BD-OCH_3 were calculated to be 210 and 112 $m^2\ g^{-1}$, respectively. The low BET surface areas were presumably attributed to hard-to-remove guest molecules trapped in the pore channels or potential porosity loss during traditional vacuum activation.[47] Furthermore, the pore size distribution of Mw-COFs was estimated from the adsorption isotherms using quenched solid density functional theory (QSDFT), revealing narrow pore width distribution centered at ∼2.3 and ∼2.2 nm for Mw-TFB-BD-CH_3 and Mw-TFB-BD-OCH_3, respectively (Figure 1B, inset). These values are close to the predicted values (2.5 and 2.3 nm) based on the eclipsed AA stacking mode.

Scanning electron microscopy (SEM) images revealed that Mw-COFs adopted uniform spherical morphologies with distinctive sizes, consistent with the results from a prior report, wherein COF spheres were formed using acetonitrile solvent.[44] Specifically, Mw-TFB-BD-CH_3 spheres had a diameter of ∼1 μm (Figures 1C and S13), whereas Mw-TFB-BD-OCH_3 and Mw-TFB-BD spheres are smaller with sizes of ∼0.7 μm and ∼0.5 μm, respectively (Figures 1D, S14, and S15). In contrast, the solvothermal counterparts of TFB-BD-CH_3 and TFB-BD-OCH_3 had dramatically different morphologies. Oven-TFB-BD-CH_3 were spherical aggregates (∼1.6 μm in diameter) consisting of irregular microparticles with sizes of 100−200 nm (Figure S16), while oven-TFB-BD-OCH_3 were nonuniform stacked nanoplates with lengths of 1−2 μm (Figure S17). Thermogravimetric analysis (TGA) profiles revealed high and different thermal stabilities of Mw-TFB-BD-X COFs under N_2 (Figure S18). Mw-TFB-BD-CH_3 and Mw-TFB-BD-OCH_3 were thermally stable up to 420 and 370 °C, respectively. Nonfunctionalized Mw-TFB-BD had the highest thermal stability with a degradation temperature of 460 °C. Besides distinctive thermal stability, the chemical stability of Mw-COFs was evaluated by exposing them to various chemical conditions. All three COFs retained long-range crystalline orders after being submersed in common organic solvents such as *n*-hexane, tetrahydrofuran, *N*, *N*-dimethylformamide (DMF), and dimethyl sulfoxide (DMSO) for 3 days (Figures S19−21). When subjected to harsh chemical environments such as boiling water (100 °C), strong acid (1 M HCl at 25 °C), and strong base (12 M NaOH at 25 °C) for 1 day, Mw-TFB-BD-CH_3 displayed higher chemical robustness than Mw-TFB-BD-OCH_3, as evidenced by the retention of major diffraction peaks in the PXRD patterns (Figures S19 and S20). Not surprisingly, Mw-TFB-BD exhibited the lowest chemical stability, with the major diffraction peaks decreasing considerably after being exposed to 1 M HCl and boiling water (Figure S21). This confirms that the introduction of electron-donating groups (−CH_3 and −OCH_3) can reinforce the hydrolytic stability of Mw-TFB-BD-CH_3 and Mw-TFB-BD-OCH_3, consistent with the previous literature.[42,43] Taken together, the forgoing characterizations not only demonstrate that the present microwave-assisted strategy enables the synthesis of COFs in a facile, rapid, and efficient manner but also prove that altering functional groups on the pore walls of Mw-TFB-BD-X COFs substantially affected the crystallinity, porosity, morphology, and thermal/chemical stability.

Enlightened by the promising structural merits of Mw-TFB-BD-CH_3/-OCH_3, including low density, high crystallinity, permanent porosity, uniform morphology, and pronounced

https://doi.org/10.1021/prechem.3c00006
Precis. Chem. 2023, 1, 233−240

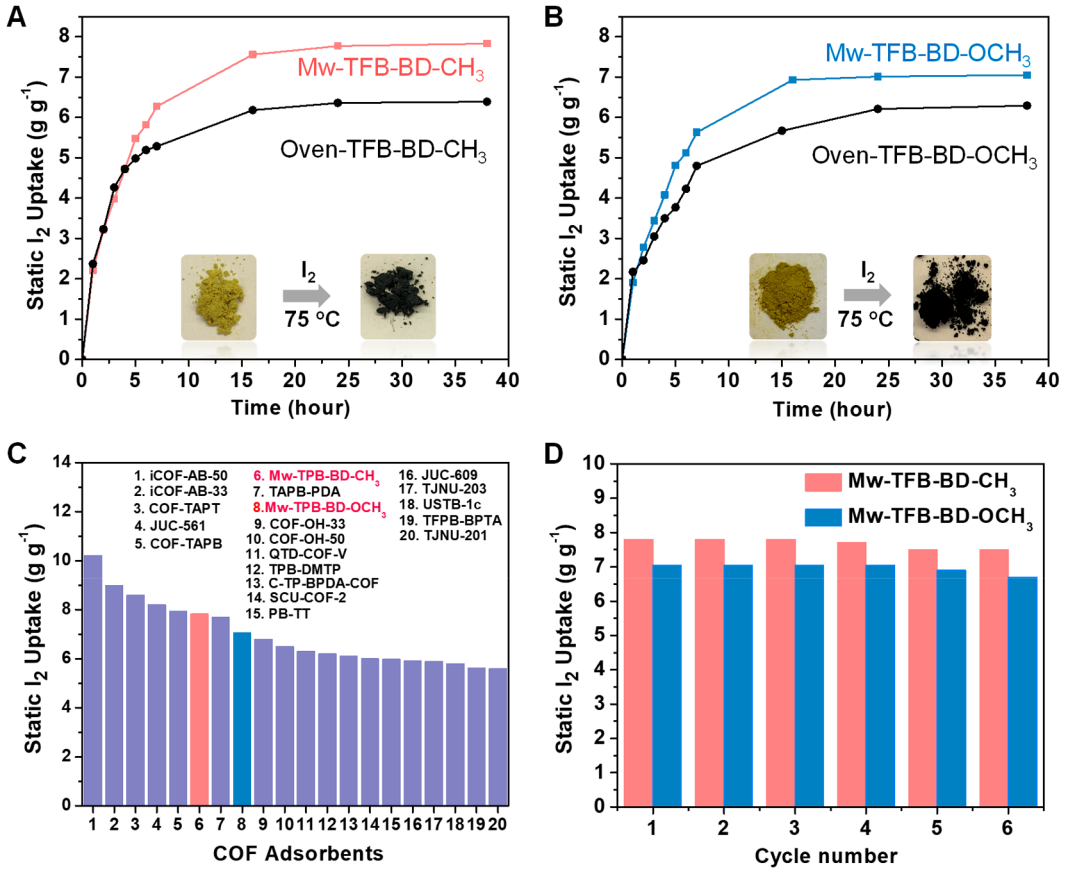

Figure 2. Time-dependent gravimetric iodine vapor adsorption of (A) Mw-TFB-BD-CH_3 and oven-TFB-BD-CH_3; (B) Mw-TFB-BD-OCH_3 and oven-TFB-BD-OCH_3 at 75 °C. Inset: Photographs of COFs before and after iodine vapor adsorption. (C) Static iodine adsorption capacities of Mw-COFs in this work and previously reported high-performing COF adsorbents (>5.0 g g^{-1}). The corresponding references are listed in Table S1; (D) Cycling performances of Mw-TFB_BD-CH_3 and Mw-TFB-BD-OCH_3.

stability, we sought to investigate their iodine capture by exposing COFs to saturated iodine vapor at 75 °C in a closed vial under static conditions. The experimental conditions are the same as those in previous studies for consistency and comparison (see the detailed experimental setup in the Supporting Information and Table S1). The iodine adsorption capacity of Mw-COFs was evaluated by time-dependent gravimetric measurements. The inset images in Figure 2A and 2B showed that the color of COF adsorbents changed from yellow to black upon exposure to the iodine vapor for 1 h, implying that gaseous iodine was adsorbed by COFs. XPS survey spectra also confirmed the iodine adsorption by COFs through intense I 3d peaks (Figure S22). Mw-TFB-BD-CH_3 revealed rapid iodine uptake in the initial stage and reached a remarkable iodine adsorption capacity of 6.27 g g^{-1} in just 7 h (Figure 2A). Similarly, Mw-TFB-BD-OCH_3 displayed rapid adsorption in the initial stage but achieved a lower iodine adsorption capacity of 5.28 g g^{-1} in 7 h (Figure 2B). Such faster kinetics and higher iodine uptake of Mw-TFB-BD-CH_3 than Mw-TFB-BD-OCH_3 may be due to its larger surface area, which facilitated the diffusion of iodine vapor within COFs. Both COFs reached adsorption saturation in 16 h. Regardless of their low surface areas (<250 m^2 g^{-1}), Mw-TFB-BD-CH_3 and Mw-TFB-BD-OCH_3 demonstrated exceptionally high iodine adsorption capacities of 7.83 g g^{-1} and 7.05 g g^{-1} at equilibrium, respectively, exceeding those of the nonfunctionalized Mw-TFB-BD (6.85 g g^{-1}, Figure S23) and their solvothermal counterparts (Figure 2A and 2B). To further evaluate their adsorption performance, we summarized the static iodine vapor adsorption capacities of reported COF adsorbents under identical or similar testing conditions (Figure 2C and Table S1). To our delight, the iodine-sorbing values render Mw-TFB-BD-CH_3 and Mw-TFB-BD-OCH_3 among the best-performing COF adsorbents in terms of adsorption capacity. It is worth noting that the synthetic route to Mw-COFs in the present study is more facile and rapid than those of existing COF adsorbents (see the detailed synthetic conditions in Table S1). Given the low surface areas of Mw-COFs, we surmise that the outstanding adsorption performance of Mw-TFB-BD-CH_3/-OCH_3 was mainly ascribed to the uniform morphology of COF spheres, which may facilitate the iodine diffusion, transport, and accessibility to the imine sites, thus positively impacting their adsorption capacity. Previous studies have shown that the morphology of adsorbents significantly influenced their adsorption performance in environmental remediation.[48−50] Noteworthy, spherical imine COFs displayed higher adsorption capacity and faster kinetics in the enrichment of peptides than those of COF counterparts with irregular morphologies.[44] In addition to exceptional capability and rapid kinetics, the iodine-captured COFs retained the iodine upon exposure to air at ambient temperature, with a negligible amount of iodine escaping from the frameworks even after 7 days, demonstrating the high adsorption stability of Mw-COFs (Figure S24).

https://doi.org/10.1021/prechem.3c00006
Precis. Chem. 2023, 1, 233−240

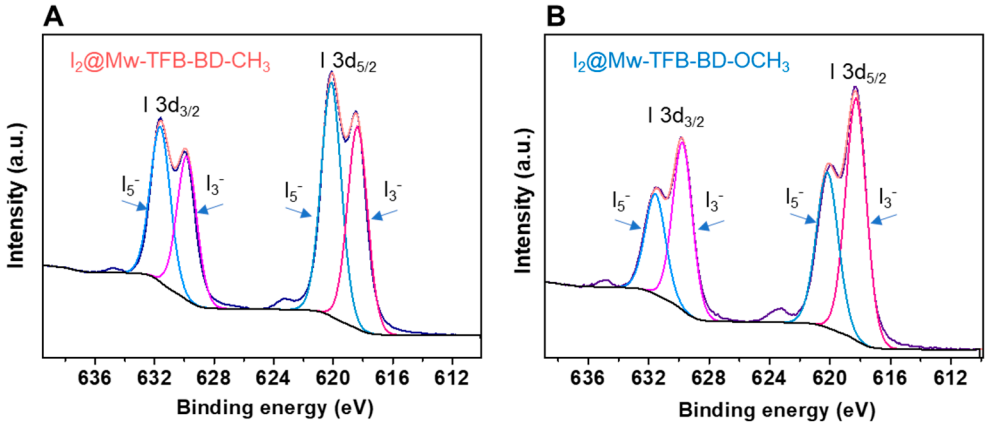

Figure 3. I 3d XPS spectra of (A) Mw-TFB-BD-CH_3 and (B) Mw-TFB-BD-OCH_3 after the iodine adsorption.

The reusability of adsorbents is the prerequisite for their practical use. To evaluate this property, we reused the Mw-COFs by facile thermal desorption of iodine-saturated COFs at 135 °C under vacuum for 20 h,[22] and then tested the regenerated COFs for their iodine adsorption capacity. Remarkably, both regenerated Mw-TFB-BD-CH_3 and Mw-TFB-BD-OCH_3 COFs retained high iodine adsorption capacities (>6.7 g g^{-1}) after 5 successive adsorption−desorption cycles (Figure 2D). PXRD analyses demonstrated that the regenerated COFs retained crystallinity after the fifth cycle, although there were noticeable decreases observed (Figure S25). Moreover, the SEM image indicated that the spherical morphology of COFs after iodine adsorption was preserved (Figure S26). The above experimental results in conjugation with prior literature demonstrate that the developed Mw-TFB-BD-CH_3 and Mw-TFB-BD-OCH_3 iodine adsorbents feature a set of intriguing features, including exceptional capacity, fast kinetics, high adsorption stability, and superb reusability, as well as rapid and facile synthesis. These properties make them highly promising for practical applications in radioiodine capture.

To shed light on the adsorption mechanism of Mw-COFs for iodine, we employed FT-IR and XPS spectroscopy to characterize COFs before and after iodine adsorption. FT-IR analysis revealed that the C═N stretching bands of I_2@Mw-TFB-BD-CH_3 showed an apparent blue shift to 1639 and 1153 cm^{-1} compared with the pristine COF (1622 and 1144 cm^{-1}). Moreover, a new band emerged at 1561 cm^{-1}, which was presumably due to the formation of C−I bonds (Figure S27).[27] FT-IR profile implied the charge transfer between imine N and iodine molecules, which was further corroborated by XPS analysis. As depicted in Figure 3A, the I 3d XPS spectra of I_2@Mw-TFB-BD-CH_3 displayed I $3d_{3/2}$ signals at 630.1 and 631.8 eV as well as I $3d_{5/2}$ signals at 618.5 and 620.1 eV, which were ascribed to the formation of triiodide (I_3^-) and pentaiodide (I_5^-) anions.[10,51−53] Based on the integral area of XPS peaks, I_3^- and I_5^- species occupy 46% and 54% of the total I_2 uptake for I_2@Mw-TFB-BD-CH_3. In contrast, I_3^- and I_5^- species take up 60% and 40% of the total I_2 uptake for I_2@Mw-TFB-BD-OCH_3 (Figure 3B), indicating the pore surface environment affected the polyiodide formation. In addition, the N 1s XPS spectra of Mw-TFB-BD-CH_3 showed two binding energy peaks at 398.3 and 399.3 eV (Figure S28A), assigned to imine N and defective amine sp^3 N. After iodine adsorption, two new peaks at 400.2 and 401.3 eV appeared, suggesting the charge transfer from various electron-rich N species to electron-deficient iodine (Figure S28B).[54] In the case of Mw-TFB-BD-OCH_3, two new N 1s peaks emerged at 400.6 and 401.6 eV(Figure S28D), indicating the formation of charge-transfer complexes between N species and iodine. These spectroscopic analyses verified the charge transfer between iodine and various N species such as imine N and defective amine sp^3 N, as well as the formation of polyiodides during the iodine adsorption process.

CONCLUSION

We have developed a facile microwave-assisted synthesis of two isoreticular imine-linked 2D COFs, Mw-TFB-BD-CH_3 and Mw-TFB-BD-OCH_3, under air within just 1 h. The resultant Mw-COFs displayed enhanced crystallinity, high yields, and uniform morphologies in comparison to their solvothermal counterparts under identical conditions. Notably, the subtle change of functional groups (−H, $-CH_3$, and $-OCH_3$) significantly influenced the crystallinity, porosity, crystallite size, and stability of Mw-COFs, offering a great platform to establish the structure-performance relationship at the atomic level. When used as adsorbents for static iodine vapor capture at 75 °C under ambient pressure, the 1-h-made Mw-TFB-BD-CH_3 and Mw-TFB-BD-OCH_3 exhibited exceptionally high iodine adsorption capacities of 7.83 g g^{-1} and 7.05 g g^{-1}, respectively, surpassing the nonfunctionalized Mw-TFB-BD, solvothermal counterparts, and most reported COF adsorbents. FT-IR and XPS analyses confirm the occurrence of chemisorption through the charge transfer between iodine and various N species in COFs. In addition, Mw-TFB-BD-CH_3 and Mw-TFB-BD-OCH_3 can be fully reused at least 5 times without obvious loss in the adsorption capacity. This work uncovers the immense potential of microwave irradiation toward the facile, rapid, and efficient synthesis of COFs for environmental remediation and beyond. Extending this strategy to the synthesis of COFs bearing novel linkages and hierarchical porosity is currently underway in our lab.

ASSOCIATED CONTENT

Supporting Information

The Supporting Information is available free of charge at https://pubs.acs.org/doi/10.1021/prechem.3c00006.

The detailed synthetic procedure, screened conditions, stability test, solvothermal control samples, simulated

https://doi.org/10.1021/prechem.3c00006
Precis. Chem. 2023, 1, 233−240

and experimental PXRD, FT-IR, TGA, SEM, XPS, and Table for the prior COF adsorbents (PDF)

AUTHOR INFORMATION

Corresponding Author

Xinle Li − *Department of Chemistry, Clark Atlanta University, Atlanta, Georgia 30314, United States;* orcid.org/0000-0001-5747-4029; Email: xli1@cau.edu

Authors

Ziad Alsudairy − *Department of Chemistry, Clark Atlanta University, Atlanta, Georgia 30314, United States*

Normanda Brown − *Department of Chemistry, Clark Atlanta University, Atlanta, Georgia 30314, United States*

Chongqing Yang − *The Molecular Foundry, Lawrence Berkeley National Laboratory, Berkeley, California 94720, United States*

Songliang Cai − *School of Chemistry, Guangzhou Key Laboratory of Analytical Chemistry for Biomedicine, South China Normal University, Guangzhou 510006, P. R. China;* orcid.org/0000-0002-5399-9036

Fazli Akram − *Department of Chemistry, Clark Atlanta University, Atlanta, Georgia 30314, United States*

Abrianna Ambus − *Department of Chemistry, Clark Atlanta University, Atlanta, Georgia 30314, United States*

Conrad Ingram − *Department of Chemistry, Clark Atlanta University, Atlanta, Georgia 30314, United States*

Complete contact information is available at: https://pubs.acs.org/10.1021/prechem.3c00006

Notes

The authors declare no competing financial interest.

ACKNOWLEDGMENTS

This research was supported by the U.S. Department of Energy Office of Science Early Career Research Program (DE-SC0022000), the National Science Foundation HBCU-UP-RIA program (no. 2100360), and the U.S. Department of Defense, the Office of Naval Research (no: N00014-20-1-2523). Part of the work was carried out at the Molecular Foundry as a user project, supported by the Office of Science, Office of Basic Energy Sciences, of the U.S. Department of Energy under Contract No. DE-AC02-05CH11231. Z.A. would like to acknowledge the support from Qassim University. S.C. is grateful for the support from the National Natural Science Foundation of China (no. 22171092).

REFERENCES

(1) Ojovan, M. I.; Steinmetz, H. J. Approaches to Disposal of Nuclear Waste. *Energies* **2022**, *15*, 7804.

(2) Riley, B. J.; Vienna, J. D.; Strachan, D. M.; McCloy, J. S.; Jerden, J. L. Materials and processes for the effective capture and immobilization of radioiodine: A review. *J. Nucl. Mater.* **2016**, *470*, 307−326.

(3) Huve, J.; Ryzhikov, A.; Nouali, H.; Lalia, V.; Augé, G.; Daou, T. J. Porous sorbents for the capture of radioactive iodine compounds: a review. *RSC Adv.* **2018**, *8*, 29248−29273.

(4) Sun, H.; La, P.; Zhu, Z.; Liang, W.; Yang, B.; Li, A. Capture and reversible storage of volatile iodine by porous carbon with high capacity. *J. Mater. Sci.* **2015**, *50*, 7326−7332.

(5) Mnasri, N.; Charnay, C.; de Ménorval, L.-C.; Moussaoui, Y.; Elaloui, E.; Zajac, J. Silver nanoparticle-containing submicron-in-size mesoporous silica-based systems for iodine entrapment and immobilization from gas phase. *Microporous Mesoporous Mater.* **2014**, *196*, 305−313.

(6) Niu, T.-H.; Feng, C.-C.; Yao, C.; Yang, W.-Y.; Xu, Y.-H. Bisimidazole-based conjugated polymers for excellent iodine capture. *ACS Appl. Polym. Mater.* **2021**, *3*, 354−361.

(7) Sun, Q.; Aguila, B.; Earl, L. D.; Abney, C. W.; Wojtas, L.; Thallapally, P. K.; Ma, S. Covalent organic frameworks as a decorating platform for utilization and affinity enhancement of chelating sites for radionuclide sequestration. *Adv. Mater.* **2018**, *30*, 1705479.

(8) Chapman, K. W.; Chupas, P. J.; Nenoff, T. M. Radioactive iodine capture in silver-containing mordenites through nanoscale silver iodide formation. *J. Am. Chem. Soc.* **2010**, *132*, 8897−8899.

(9) Zhang, X.; Maddock, J.; Nenoff, T. M.; Denecke, M. A.; Yang, S.; Schröder, M. Adsorption of iodine in metal−organic framework materials. *Chem. Soc. Rev.* **2022**, *51*, 3243−3262.

(10) Liu, C.; Jin, Y.; Yu, Z.; Gong, L.; Wang, H.; Yu, B.; Zhang, W.; Jiang, J. Transformation of Porous Organic Cages and Covalent Organic Frameworks with Efficient Iodine Vapor Capture Performance. *J. Am. Chem. Soc.* **2022**, *144*, 12390−12399.

(11) Zhang, L.; Jin, Y.; Tao, G. H.; Gong, Y.; Hu, Y.; He, L.; Zhang, W. Desymmetrized vertex design toward a molecular cage with unusual topology. *Angew. Chem., Int. Ed.* **2020**, *59*, 20846−20851.

(12) Hasell, T.; Schmidtmann, M.; Cooper, A. I. Molecular doping of porous organic cages. *J. Am. Chem. Soc.* **2011**, *133*, 14920−14923.

(13) Diercks, C. S.; Yaghi, O. M. The atom, the molecule, and the covalent organic framework. *Science* **2017**, *355*, eaal1585.

(14) Geng, K.; He, T.; Liu, R.; Dalapati, S.; Tan, K. T.; Li, Z.; Tao, S.; Gong, Y.; Jiang, Q.; Jiang, D. Covalent organic frameworks: design, synthesis, and functions. *Chem. Rev.* **2020**, *120*, 8814−8933.

(15) Li, X.; Wang, H.; Chen, H.; Zheng, Q.; Zhang, Q.; Mao, H.; Liu, Y.; Cai, S.; Sun, B.; Dun, C.; et al. Dynamic covalent synthesis of crystalline porous graphitic frameworks. *Chem* **2020**, *6*, 933−944.

(16) Li, X.; Zhang, C.; Cai, S.; Lei, X.; Altoe, V.; Hong, F.; Urban, J. J.; Ciston, J.; Chan, E. M.; Liu, Y. Facile transformation of imine covalent organic frameworks into ultrastable crystalline porous aromatic frameworks. *Nat. Commun.* **2018**, *9*, 2998.

(17) Tang, X.; Liao, X.; Cai, X.; Wu, J.; Wu, X.; Zhang, Q.; Yan, Y.; Zheng, S.; Jiang, H.; Fan, J.; Cai, S.; Zhang, W.; Liu, Y. Self-Assembly of Helical Nanofibrous Chiral Covalent Organic Frameworks. *Angew. Chem., Int. Ed.* **2023**, *62*, e202216310.

(18) Yang, C.; Jiang, K.; Zheng, Q.; Li, X.; Mao, H.; Zhong, W.; Chen, C.; Sun, B.; Zheng, H.; Zhuang, X.; et al. Chemically Stable Polyarylether-Based Metallophthalocyanine Frameworks with High Carrier Mobilities for Capacitive Energy Storage. *J. Am. Chem. Soc.* **2021**, *143*, 17701−17707.

(19) Yin, Z.-J.; Xu, S.-Q.; Zhan, T.-G.; Qi, Q.-Y.; Wu, Z.-Q.; Zhao, X. Ultrahigh volatile iodine uptake by hollow microspheres formed from a heteropore covalent organic framework. *Chem. Commun.* **2017**, *53*, 7266−7269.

(20) Wang, P.; Xu, Q.; Li, Z.; Jiang, W.; Jiang, Q.; Jiang, D. Exceptional iodine capture in 2D covalent organic frameworks. *Adv. Mater.* **2018**, *30*, 1801991.

(21) Yan, X.; Yang, Y.; Li, G.; Zhang, J.; He, Y.; Wang, R.; Lin, Z.; Cai, Z. Thiophene-based covalent organic frameworks for highly efficient iodine capture. *Chin. Chem. Lett.* **2023**, *34*, 107201.

(22) Yang, Y.-X.; Tang, X.-H.; Wu, J.-L.; Dong, Z.-Y.; Yan, Y.-L.; Zheng, S.-R.; Fan, J.; Li, X.; Cai, S.; Zhang, W.-G. Transformation of a hydrazone-linked covalent organic framework into a highly stable hydrazide-linked one. *ACS Appl. Polym. Mater.* **2022**, *4*, 4624−4631.

(23) Li, Y.; Li, X.; Li, J.; Cheng, G.; Ke, H.; et al. Phosphine-based covalent organic framework for highly efficient iodine capture. *Microporous Mesoporous Mater.* **2021**, *325*, 111351.

(24) Zhang, S.-Y.; Tang, X.-H.; Yan, Y.-L.; Li, S.-Q.; Zheng, S.; Fan, J.; Li, X.; Zhang, W.-G.; Cai, S. Facile and Site-Selective Synthesis of an Amine-Functionalized Covalent Organic Framework. *ACS Macro Lett.* **2021**, *10*, 1590−1596.

(25) Zhai, L.; Sun, S.; Chen, P.; Zhang, Y.; Sun, Q.; Xu, Q.; Wu, Y.; Nie, R.; Li, Z.; Mi, L. Constructing cationic covalent organic frameworks by a post-function process for an exceptional iodine

capture via electrostatic interactions. *Mater. Chem. Front.* **2021**, *5*, 5463−5470.
(26) Yang, Y.; Tu, C.; Yin, H.; Liu, J.; Cheng, F.; Luo, F. Molecular Iodine Capture by Covalent Organic Frameworks. *Molecules* **2022**, *27*, 9045.
(27) Xie, Y.; Pan, T.; Lei, Q.; Chen, C.; Dong, X.; Yuan, Y.; Shen, J.; Cai, Y.; Zhou, C.; Pinnau, I.; et al. Ionic Functionalization of Multivariate Covalent Organic Frameworks to Achieve an Exceptionally High Iodine-Capture Capacity. *Angew. Chem., Int. Ed.* **2021**, *60*, 22432−22440.
(28) Chang, J.; Li, H.; Zhao, J.; Guan, X.; Li, C.; Yu, G.; Valtchev, V.; Yan, Y.; Qiu, S.; Fang, Q. Tetrathiafulvalene-based covalent organic frameworks for ultrahigh iodine capture. *Chem. Sci.* **2021**, *12*, 8452−8457.
(29) Zhu, D.; Zhu, Y.; Yan, Q.; Barnes, M.; Liu, F.; Yu, P.; Tseng, C.-P.; Tjahjono, N.; Huang, P.-C.; Rahman, M. M.; Egap, E.; Ajayan, P. M.; Verduzco, R. Pure Crystalline Covalent Organic Framework Aerogels. *Chem. Mater.* **2021**, *33*, 4216−4224.
(30) Wang, C.; Wang, Y.; Ge, R.; Song, X.; Xing, X.; Jiang, Q.; Lu, H.; Hao, C.; Guo, X.; Gao, Y.; Jiang, D. A 3D Covalent Organic Framework with Exceptionally High Iodine Capture Capability. *Chem. Eur. J.* **2018**, *24*, 585−589.
(31) Emmerling, S. T.; Germann, L. S.; Julien, P. A.; Moudrakovski, I.; Etter, M.; Friščić, T.; Dinnebier, R. E.; Lotsch, B. V. In situ monitoring of mechanochemical covalent organic framework formation reveals templating effect of liquid additive. *Chem.* **2021**, *7*, 1639−1652.
(32) Zhang, M.; Chen, J.; Zhang, S.; Zhou, X.; He, L.; Sheridan, M. V.; Yuan, M.; Zhang, M.; Chen, L.; Dai, X.; et al. Electron beam irradiation as a general approach for the rapid synthesis of covalent organic frameworks under ambient conditions. *J. Am. Chem. Soc.* **2020**, *142*, 9169−9174.
(33) Zhao, W.; Yan, P.; Yang, H.; Bahri, M.; James, A. M.; Chen, H.; Liu, L.; Li, B.; Pang, Z.; Clowes, R.; et al. Using sound to synthesize covalent organic frameworks in water. *Nat. Syn.* **2022**, *1*, 87−95.
(34) Li, X.; Yang, C.; Sun, B.; Cai, S.; Chen, Z.; Lv, Y.; Zhang, J.; Liu, Y. Expeditious synthesis of covalent organic frameworks: a review. *J. Mater. Chem. A* **2020**, *8*, 16045−16060.
(35) Nüchter, M.; Ondruschka, B.; Bonrath, W.; Gum, A. Microwave assisted synthesis−a critical technology overview. *Green Chem.* **2004**, *6*, 128−141.
(36) Campbell, N. L.; Clowes, R.; Ritchie, L. K.; Cooper, A. I. Rapid microwave synthesis and purification of porous covalent organic frameworks. *Chem. Mater.* **2009**, *21*, 204−206.
(37) Diaz de Grenu, B.; Torres, J.; García-González, J.; Muñoz-Pina, S.; De los Reyes, R.; Costero, A. M.; Amorós, P.; Ros-Lis, J. V. Microwave-Assisted Synthesis of Covalent Organic Frameworks: A Review. *ChemSusChem* **2021**, *14*, 208−233.
(38) Li, Y.; Chen, W.; Xing, G.; Jiang, D.; Chen, L. New synthetic strategies toward covalent organic frameworks. *Chem. Soc. Rev.* **2020**, *49*, 2852−2868.
(39) Feriante, C. H.; Jhulki, S.; Evans, A. M.; Dasari, R. R.; Slicker, K.; Dichtel, W. R.; Marder, S. R. Rapid Synthesis of High Surface Area Imine-Linked 2D Covalent Organic Frameworks by Avoiding Pore Collapse During Isolation. *Adv. Mater.* **2020**, *32*, 1905776.
(40) Hu, J.; Gupta, S. K.; Ozdemir, J.; Beyzavi, H. Applications of dynamic covalent chemistry concept toward tailored covalent organic framework nanomaterials: A review. *ACS Appl. Nano Mater.* **2020**, *3*, 6239−6269.
(41) Alahakoon, S. B.; Diwakara, S. D.; Thompson, C. M.; Smaldone, R. A. Supramolecular design in 2D covalent organic frameworks. *Chem. Soc. Rev.* **2020**, *49*, 1344−1356.
(42) Xu, H.; Gao, J.; Jiang, D. Stable, crystalline, porous, covalent organic frameworks as a platform for chiral organocatalysts. *Nat. Chem.* **2015**, *7*, 905−912.
(43) Tao, S.; Zhai, L.; Dinga Wonanke, A.; Addicoat, M. A.; Jiang, Q.; Jiang, D. Confining H3PO4 network in covalent organic frameworks enables proton super flow. *Nat. Commun.* **2020**, *11*, 1981.
(44) Ma, W.; Zheng, Q.; He, Y.; Li, G.; Guo, W.; Lin, Z.; Zhang, L. Size-controllable synthesis of uniform spherical covalent organic frameworks at room temperature for highly efficient and selective enrichment of hydrophobic peptides. *J. Am. Chem. Soc.* **2019**, *141*, 18271−18277.
(45) Li, R. L.; Flanders, N. C.; Evans, A. M.; Ji, W.; Castano, I.; Chen, L. X.; Gianneschi, N. C.; Dichtel, W. R. Controlled growth of imine-linked two-dimensional covalent organic framework nanoparticles. *Chem. Sci.* **2019**, *10*, 3796−3801.
(46) Smith, B. J.; Overholts, A. C.; Hwang, N.; Dichtel, W. R. Insight into the crystallization of amorphous imine-linked polymer networks to 2D covalent organic frameworks. *Chem. Commun.* **2016**, *52*, 3690−3693.
(47) Zhu, D.; Verduzco, R. Ultralow surface tension solvents enable facile COF activation with reduced pore collapse. *ACS Appl. Mater. Interfaces* **2020**, *12*, 33121−33127.
(48) Huang, J.; Cao, Y.; Shao, Q.; Peng, X.; Guo, Z. Magnetic Nanocarbon Adsorbents with Enhanced Hexavalent Chromium Removal: Morphology Dependence of Fibrillar vs Particulate Structures. *Ind. Eng. Chem. Res.* **2017**, *56*, 10689−10701.
(49) Jeon, S.; Yong, K. Morphology-controlled synthesis of highly adsorptive tungsten oxide nanostructures and their application to water treatment. *J. Mater. Chem.* **2010**, *20*, 10146−10151.
(50) Zhao, S.; Kang, D.; Yang, Z.; Huang, Y. Facile synthesis of iron-based oxide from natural ilmenite with morphology controlled adsorption performance for Congo red. *Appl. Surf. Sci.* **2019**, *488*, 522−530.
(51) Li, X.; Xiong, H.; Jia, Q. A Versatile Solvent-Induced Polymerization Strategy To Synthesize Free-Standing Porous Polymer Nanosheets and Nanotubes for Fast Iodine Capture. *ACS Appl. Mater. Interfaces* **2019**, *11*, 46205−46211.
(52) Harijan, D. K. L.; Chandra, V.; Yoon, T.; Kim, K. S. Radioactive iodine capture and storage from water using magnetite nanoparticles encapsulated in polypyrrole. *J. Hazard. Mater.* **2018**, *344*, 576−584.
(53) Li, X.; Jia, Z.; Zhang, J.; Zou, Y.; Jiang, B.; Zhang, Y.; Shu, K.; Liu, N.; Li, Y.; Ma, L. Moderate and Universal Synthesis of Undoped Covalent Organic Framework Aerogels for Enhanced Iodine Uptake. *Chem. Mater.* **2022**, *34*, 11062−11071.
(54) Xie, W.; Cui, D.; Zhang, S.-R.; Xu, Y.-H.; Jiang, D.-L. Iodine capture in porous organic polymers and metal−organic frameworks materials. *Mater. Horiz.* **2019**, *6*, 1571−1595.

https://doi.org/10.1021/prechem.3c00006
Precis. Chem. 2023, 1, 233−240